Development of next generation LLRF control system for J-PARC rapid cycling synchrotron

Fumihiko Tamura, Yasuyuki Sugiyama, Masahito Yoshii, Masatsugu Ryoshi

***Abstract*—The low level rf (LLRF) control system for the rapid cycling synchrotron (RCS) of the Japan Proton Accelerator Research Complex (J-PARC) started its operation in 2007. The key functions of the LLRF control system are the dual harmonic auto voltage control, which generates superposed voltages of the fundamental accelerating harmonic and the second harmonic in a single wideband magnetic alloy (MA) cavity, and the multiharmonic rf feedforward to compensate the beam loading in the MA cavity caused by high intensity beams. These functions are necessary to accelerate high intensity proton beams. The system has been working well without major problems for more than ten years. However, the old FPGAs (Xilinx Virtex-II pro etc.) are discontinued and not supported by the current development environment. It will be difficult to maintain the system in near future. Thus, we are planning to replace the existing VME-based LLRF control system with a new MicroTCA.4 based system. The system controls twelve cavities independently and calculates vector sum of the cavity voltages in real time for phase feedback. Signal and data transfer between the modules is a key to realize the functions. In the existing system, the transfer is implemented not only the backplane but also serial link via cables between the VME modules. It is much more simplified in the new system thanks to the high speed communication capability of the MicroTCA.4 backplane. In this article, we describe the configuration of the system under development, the implemented functions, and preliminary test results.**

***Index Terms*—Proton Synchrotron, Low level rf (LLRF), field-programmable gate array (FPGA), MicroTCA.4**

I. Introduction

The rapid cycling synchrotron (RCS) in the Japan Proton Accelerator Research Complex (J-PARC) [1] acts as a high intensity proton driver, which delivers high intensity proton beams to the Material and Life Science Experimental Facility (MLF) for generation of neutrons and muons, as well as the injector for the main ring synchrotron (MR). The design output beam power of the RCS is 1 MW.

The beam commissioning of the RCS started in October 2007 and the output beam power has been steadily increasing with progress of the beam tuning and hardware upgrades. During the high intensity beam study performed in January 2015, 8.3×10^{13} protons, which corresponds to the beam power of 1 MW at the repetition rate of 25 Hz, were successfully accelerated with a low beam loss below 0.2% [2]. The demonstration was performed in the single shot mode, where a beam pulse is injected from the linac to the RCS on demand. As of May 2018, the output beam power for the MLF is 500 kW and the RCS delivers 6.5×10^{13} ppp to the MR.

A schematic view of the RCS is shown in Fig. 1, and the parameters of the RCS and its rf system are listed in Table I. A 400 MeV H^- beam is injected and converted to a proton beam by a charge exchange foil. To avoid longitudinal beam losses, the injected beam has a chopped structure synchronized to the RCS rf voltage. The RCS accelerates the protons up to 3 GeV in 20 ms with the repetition rate of 25 Hz. As shown in Fig. 1, the RCS has a three-fold symmetry. The three straight sections are dedicated for the injection devices and the collimators, the extraction devices, and the rf systems.

Twelve magnetic ally (MA) cavities are installed in the RCS to generate the high accelerating voltage of 440 kV maximum for acceleration of high intensity proton beams. The cavities are driven by tetrode tube amplifiers. The MA cavity has a wideband frequency response ($Q = 2$), which covers not only

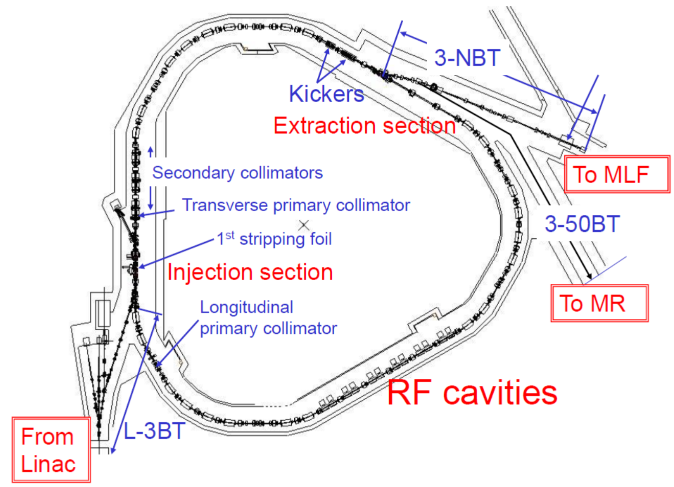

Fig. 1. Schematic view of the J-PARC RCS.

TABLE I
PARAMETERS OF THE J-PARC RCS AND ITS RF SYSTEM

parameter	
circumference	348.333 m
energy	0.400–3 GeV
beam intensity	(achieved) 8.3×10^{13} ppp
harmonic number	2
accelerating frequency	1.227–1.671 MHz
maximum rf voltage	440 kV
repetition rate	25 Hz
No. of cavities	12
Q-value of rf cavity	2

Manuscript received June 15, 2018

Fumihiko Tamura, Yasuyuki Sugiyama and Masahito Yoshii are with the J-PARC Center, JAEA & KEK, 2-4 Shirakata, Tokai, Ibaraki 319-1195, Japan. (e-mail: fumihiko.tamura@j-parc.jp)

Masatsugu Ryoshi is with Mitsubishi Electric TOKKI systems Corporation, 4-11 Techno Park, Sanda, Hyogo 669-1339, Japan

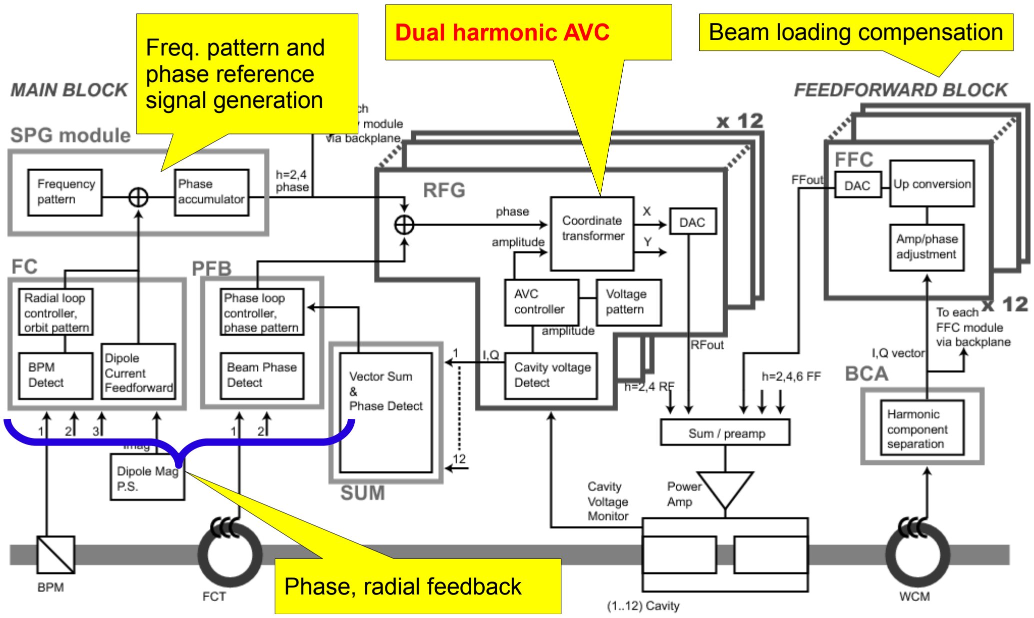

Fig. 2. Block diagram of the existing LLRF control system.

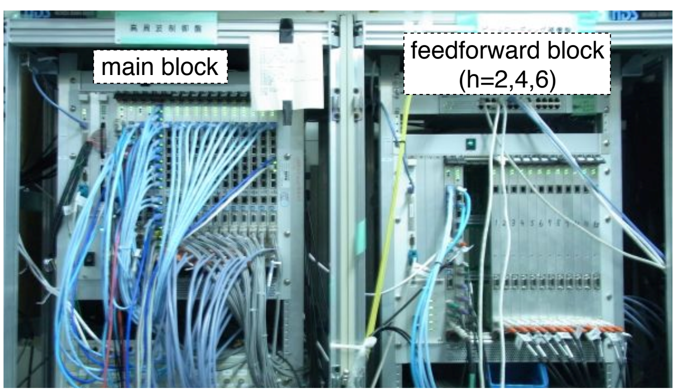

Fig. 3. Photo of the existing LLRF control system.

the wide accelerating ($h = 2$) frequency sweep to follow the velocity change of the proton beam during acceleration without a tuning bias loop, but also the frequency range of the second harmonic ($h = 4$). The wideband frequency response enables the dual harmonic operation, where each cavity is driven by the superposition of the fundamental and second harmonic rf voltages for bunch shaping. The bunch shaping with the dual harmonic operation is indispensable for alleviating the space charge effects of the high intensity proton beams.

The beam loading in the cavity [3] is a key issue for accelerating high intensity proton beams. In case of the wideband MA cavity, the wake voltage consists of not only the accelerating harmonic, but also the higher harmonics. A multiharmonic beam loading compensation is necessary.

These functions and other functions are implemented in the low level rf (LLRF) control system. The LLRF control system is a key for stable acceleration of high intensity protons. The existing LLRF control system started its operation in 2007 from the beginning of the beam commissioning and operation of the J-PARC RCS. After a decade of operation, a next generation LLRF system for the RCS is under development. In this article, we describe the configuration of the new system.

II. Existing LLRF control system

A. *Configuration and functions*

The functional block diagram and the photograph are shown in Fig. 2 and Fig. 3 respectively. Specialized 9U height VME modules were developed to realize the functions. The P1 connector is connected to the normal VME bus and the P2 and P3 connectors are specialized ones dedicated for the signal transfer between the modules. All functions are implemented as logic circuits on FPGA, Xilinx Virtex-II pro and Spartan-2. The system clock frequency is 36 MHz.

To realize the frequency sweep, a frequency pattern memory is implemented in a module. The revolution frequency signal is fed to a phase accumulator to generate the revolutional phase signal from $-\pi$ to π. The phase signals of the higher harmonics are generated by multiplying the revolutional phase signal by the harmonic number h, therefore the synchronization between the revolutional and higher harmonics is guaranteed. The multiharmonic phase signals are distributed to all modules via the backplane. By using the phase signals, synchronization of the modules for all cavities is also guaranteed. Sinusoidal signals for the I/Q demodulation and modulation of the rf and beam signals are generated from the phase signals.

Since the frequency range of the cavity and beam signals is relatively low, MHz range, no additional analog parts for down and up conversion are necessary; the beam or cavity signal is directly digitized by ADCs and cavity driving signal is generated by DACs.

The main role of the system is the regulation of the cavity voltages. Each cavity has the dual harmonic auto voltage control (AVC) loop [4]. In the dual harmonic AVC, the I/Q signals of the accelerating ($h = 2$) and the second harmonic ($h = 4$)

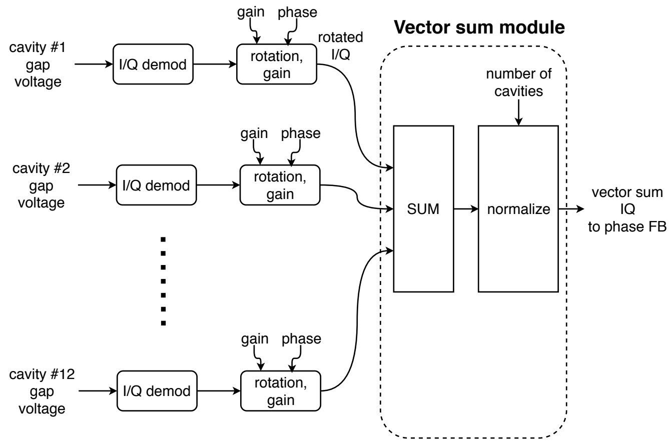

Fig. 4. Schematic diagram of the vector sum.

voltages are converted to the amplitudes. The amplitudes are compared to the voltage patterns and via PI controllers, the AVC outputs the amplitude control signal. Finally, from the amplitudes and the phase signals of the harmonics ($h = 2, 4$), the dual harmonic rf signal is generated. The longitudinal painting injection [5] is achieved by using the dual harmonic AVC.

The other important function for the high intensity acceleration is the multiharmonic beam loading compensation. The rf feedforward method is employed in the existing system [6]. The feedforward system picks up the complex amplitude of the beam signal for the selected harmonic. The gain and phase is set so that the feedforward signal cancels the wake voltage in the cavity. We developed the commissioning methodology of the multiharmonic feedforward system [6]. Originally the feedforward system for the even harmonics ($h = 2, 4, 6$) was installed and commissioned, and the additional feedforward system for the odd harmonics ($h = 1, 3, 5$) was installed for the high intensity single bunch operation [7].

The feedback loops to stabilize the beam are also implemented.

The radial loop modulates the frequency using the beam position monitor (BPM) signal so that the beam orbit is centered in the bending magnets. The radial feedback is not used, because the reproducibilities of the bending field and the rf frequency good enough.

The phase feedback modulates the phases of the cavity voltages to damp the longitudinal dipole oscillation. It compares the beam phase and the phase of the vector sum of the cavity voltages. In Fig. 4, the block diagram of the vector sum function is illustrated. The detected I/Q cavity voltage of the harmonic is rotated and sent to the vector sum module. The rotation angle is set corresponding to the cavity position in the RCS ring. Optionally a gain can be applied to the I/Q signal. The summation signal is normalized by using the number of cavities and sent to the phase feedback module.

The miscellaneous functions not shown in the figure, such as generation of the trigger pulse for the extraction kicker magnets and generation of the linac chopper pulse, are also implemented.

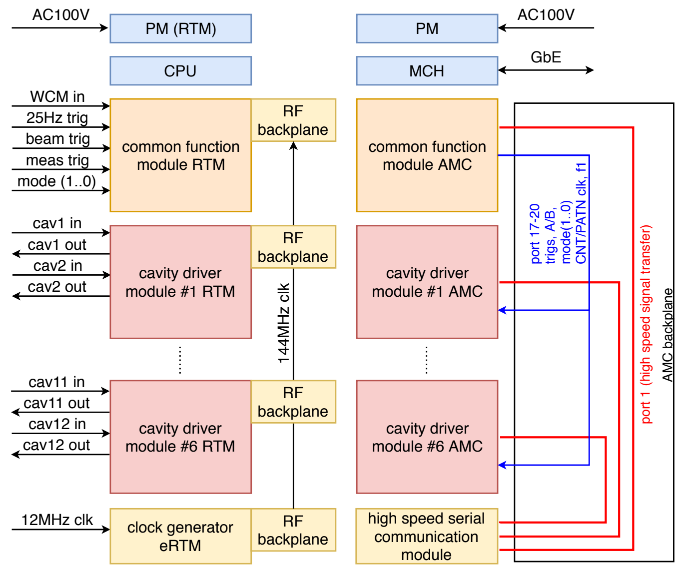

Fig. 5. Configuration of the next generation LLRF control system.

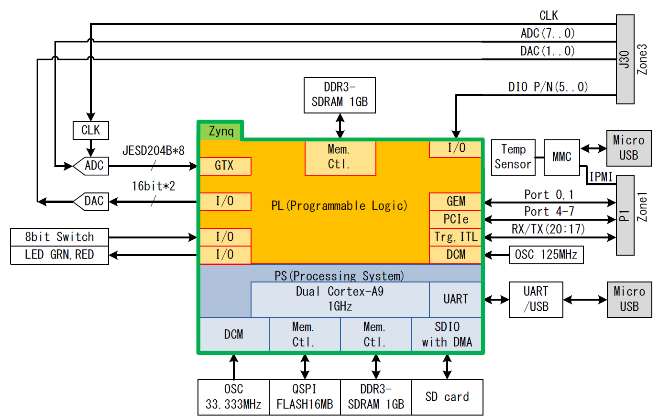

Fig. 6. Functional block diagram of the AMC module for the next generation LLRF control system.

B. Demand of the next generation system

The existing LLRF control system started its operation in 2007, and has been working well without major problems for more than ten years. The dual harmonic AVC, multiharmonic feedforward and the other LLRF functions serve the high intensity beam operation. However, the old FPGAs (Xilinx Virtex-II pro and others) used in the modules are already discontinued and not supported by the current development environment. Although we have several spare modules, it will be difficult to maintain the existing system in near future. Therefore, we decided to develop a next generation LLRF control system.

Since we developed the existing modules by analogy of analog LLRF modules, the module design is different for each of the functions. Maintenance of the spare modules is a practical issue. More generic configuration, the generic FPGA board and additional I/O board for example, is preferable for the new system.

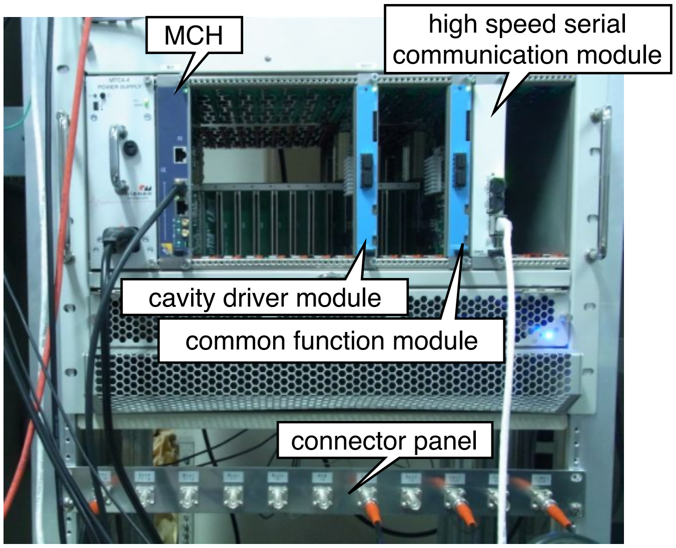

Fig. 7. Photograph of the next generation LLRF control system.

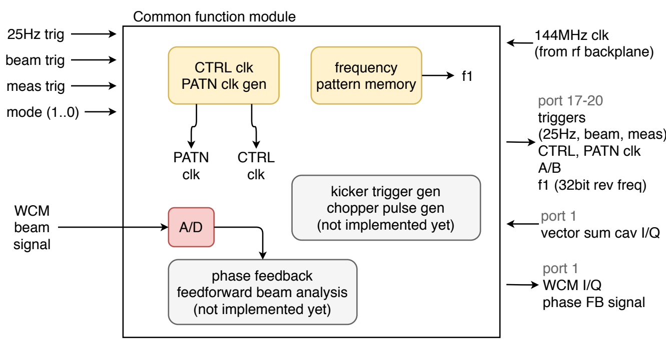

Fig. 8. Block diagram of the common function module.

III. Next generation LLRF control system

A. System overview

We employ the MicroTCA.4 platform for the next generation LLRF control system. Separation of the I/Os in rear transition modules (RTM) and the FPGA logic in AMC modules gives us design flexibility.

The configuration of the system is shown in Fig. 5. The clock generator eRTM generates the 144 MHz system clock from the J-PARC master clock of 12 MHz by using a phase lock loop. The DESY-type rf backplane is utilized for system clock distribution to the modules.

The general purpose AMC module developed by Mitsubishi Electric TOKKI Systems Corporation is employed. The block diagram of the AMC board is shown in Fig. 6. It has a modern SoC FPGA, Xilinx Zynq XC7Z045, where an EPICS IOC with Linux is embedded. Setting and monitoring of the parameters are done via EPICS channel access. The EPICS waveform records of I/Q signals are useful for commissioning of the system. The 1 GB SDRAM is used as pattern memories. It has eight high speed ADCs and two DACs, i.e. it has capability to control two cavities. Also, it has 6-bit digital I/O. The RTM are developed for the specific I/O and functions.

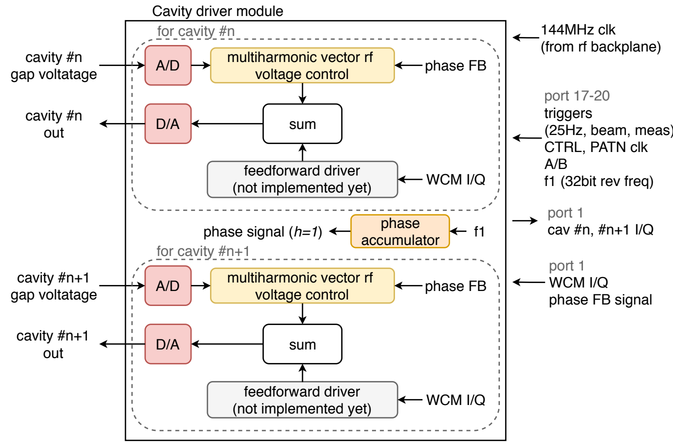

Fig. 9. Block diagram of the cavity driver module.

We classify the LLRF functions into the categories, “common function” and “cavity driving function”, which are implemented the common function modules and the cavity driver modules, respectively. A high speed serial communication module is located in the slot of MCH2.

A photograph of the next generation LLRF control system is shown in Fig. 7. In JFY 2017, one common function module, one cavity driver module, the clock generator eRTM, and the high speed serial communication module were constructed.

B. Common function module

A functional block diagram of the common function module is illustrated in Fig. 8. The common function module manages the revolutional frequency pattern, the phase feedback to damp the longitudinal oscillations, and other functions. The common function module receives the triggers and the information of the RCS beam destination, “mode (1..0)”, as shown in Fig. 5. The common function module generates the control clock used in the feedback blocks and the pattern clock for pattern sampling. Frequencies of the clocks can be set independently. They are set to 1 MHz for this application. These clocks and informations are distributed to the cavity driver modules via the AMC backplane. The 32-bit revolutional frequency signal from the pattern memory is serialized and distributed, while the existing system distributes the phase signals of the accelerating ($h = 2$) and the second harmonic ($h = 4$). The cavity driver module has its own phase accumulator and multiplier to generate the multiharmonic phase signals. This configuration is necessary for the multiharmonic vector rf voltage control described below.

At present, the phase feedback, the beam signal analysis for rf feedforward, the kicker trigger generation, and the chopper pulse generation, are not implemented yet. The radial feedback is not to be implemented based on our experience with the existing system.

C. Cavity driver module

A functional block diagram is shown in Fig. 9. As described above, it handles two cavity voltages independently by using

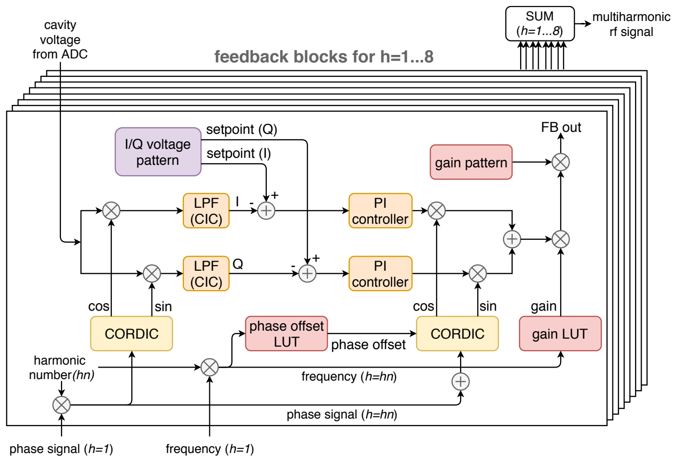

Fig. 10. Block diagram of the multiharmonic vector rf voltage control.

two ADCs and two DACs. Six cavity driver modules are necessary to control twelve cavity voltages, while one module is constructed in JFY 2017.

The revolutional frequency signal from the backplane is led to the phase accumulator to generate the phase signal, which is multiplied by the harmonic numbers in the function blocks to generate the multiharmonic phase signal. The functions of the cavity driver are the multiharmonic vector rf voltage control and the feedforward driver. Available logic cells of the Zynq FPGA are much more than that of old FPGAs used in the existing system; now these functions for two cavities can be implemented in a single FPGA.

The feedforward driver receives the I/Q amplitudes of the beam signal for the selected harmonics and generates the feedforward compensation signal similarly to the existing rf feedforward system. The feedforward driver is not implemented yet. The number of harmonics is to be extended from six of the existing system to eight.

The multiharmonic vector rf voltage control is the key function of the next generation LLRF control system. In the existing system, the amplitudes of two harmonics ($h = 2, 4$) are controlled. The new system can control the I/Q complex amplitudes of eight harmonics ($h = 1...8$). By controlling the complex amplitudes, the beam loading is compensated and the phase control of the higher harmonics is possible.

The block consists of eight feedback blocks as shown in Fig. 10. The I/Q complex amplitude of the cavity voltage signal is obtained by I/Q demodulation. A narrow band CIC (cascaded integrator and comb) filter is used as a low pass filter. The complex amplitude is compared to the I/Q voltage pattern. Through the PI controller and the I/Q modulator, feedback output is obtained.

The revolutional frequency signal and the phase signal are multiplied by the harmonic number (hn) in the feedback block to obtain the frequency and the phase signal of the selected harmonic number (hn), respectively. The sine and cosine signals for the I/Q demodulator and modulator are generated by the CORDIC using the phase signal of the harmonic. The frequency signal is used for addressing of the phase offset LUT and the gain LUT. The phase offset LUT gives

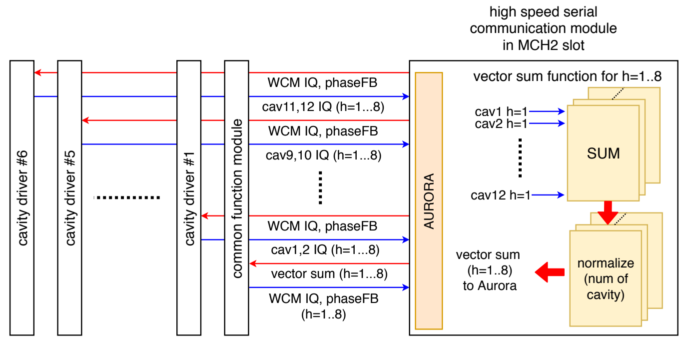

Fig. 11. Block diagram of the high speed serial communication module and the signal flow around the modules.

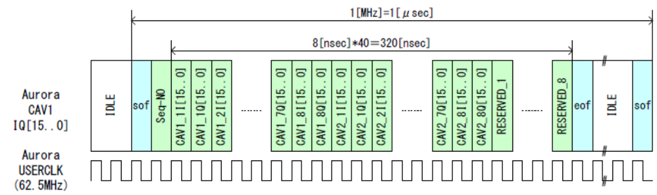

Fig. 12. Data format for the cavity I/Q signals.

a phase offset between the I/Q demodulator and modulator to adjust the phase of the 1-turn transfer function. The gain LUT compensates the amplitude response of the cavity. These LUTs are necessary to cover the wide frequency range.

Finally, eight rf signals from the feedback blocks are summed up to obtain the multiharmonic rf signal.

D. High speed serial communication module

Signal transfer between the modules is a key to realize the LLRF functions. Actually, the signal transfer of the existing system is not very sophisticated; parallel bus connection in the backplane is used for distribution of the multiharmonic phase signal and the cavity I/Q voltages are sent to the vector sum module by serial link via cables across the front panels of the modules, as shown in the photograph in Fig. 2.

The signal transfers required by the LLRF functions are as follows.

- I/Q amplitudes of the cavity voltages for the all harmonics from the cavity drivers to the vector sum function
- I/Q amplitudes of the WCM beam signal from the common function module to the cavity driver modules
- phase feedback signal from the common function module to the cavity driver modules

One can see that all of the transfers are star topologies. A star topology can be implemented by using the port 1 connections of the AMC backplane and installing a dedicated module in the slot for MCH2, while the configuration sacrifices the redundancy.

The block diagram of the high speed serial communication module and the signal flow around the module are illustrated in Fig. 11. The cavity driver module sends the I/Q amplitudes of the two cavities for eight harmonics ($h = 1..8$), which are

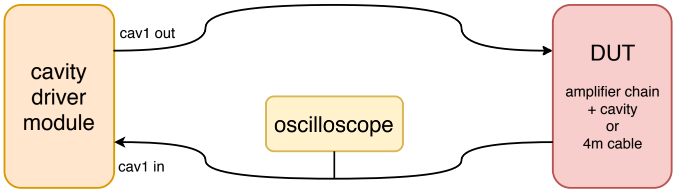

Fig. 13. Test setup of the cavity driver module.

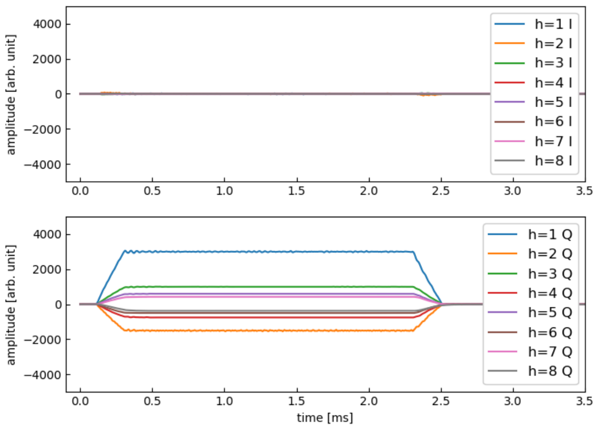

Fig. 14. Measured I/Q amplitudes of eight harmonics ($h = 1..8$).

rotated according to the position in the tunnel, to the communication module. To realize a number of serial connections, Xilinx Virtex-5 is employed. The Xilinx Aurora protocol is employed for the signal transfer. The data format for the cavity I/Q signals is shown in Fig. 12. The data rate is set to 2.5 Gbps and a single data frame contains 40 data blocks. Therefore, the time width of the frame is 320 ns. In case of the I/Q signals for two cavities, 32 data blocks are actually used. The data frame is sent every control clock cycle, 1 μs.

In the communication module, the vector sum function similar to Fig. 4. The I/Q amplitudes from the cavity drivers are summed up and normalized by the number of cavities. The vector sum of the all harmonics is sent to the common function module and it is used for the phase feedback loop.

The I/Q amplitudes of the WCM beam signal for eight harmonics and the phase feedback signal are sent from the common function module to the communication module. The communication module distribute the signals to all cavity drivers.

Thanks to the capability of the AMC backplane for the high speed serial communication, the signal transfer between the LLRF modules is much more sophisticated and simplified than the existing system.

IV. Preliminary Test Results

A. Multiharmonic vector rf control

The test setup of the cavity driver module is shown in Fig. 13. The rf output for the cavity 1 is led to the DUT (device under test) and the output of the DUT is fed into the cavity 1 input of the driver module. The DUT is the amplifier chain and the cavity. The phase offset LUT was set so that the feedback loop can be closed.

To demonstrate the performance of the multiharmonic vector rf control, a sawtooth wave is generated. The Fourier series $f(t)$ of a sawtooth wave with a frequency f_1 and the amplitude 1 up to m-th harmonic is

$$f(t) = \frac{2}{\pi} \sum_{h=1}^{m} \frac{(-1)^{h+1}}{h} \sin 2\pi h f_1 t, \tag{1}$$

where h is the harmonic number. The module can control eight harmonics ($h = 1..8$). In the test, f_1 was set to 1 MHz and the I/Q amplitude of the revolutional harmonic ($h = 1$) is set to (0,3000), which are digital values. The amplitudes of the higher harmonics are set according to (1).

The measured I/Q signals of the eight harmonics ($h = 1..8$) and the comparison of the measured and calculated cavity gap voltage waveforms are plotted in Fig. 14 and Fig. 15, respectively. One can see that the I/Q amplitudes of the harmonics are very close to the set points. The measured and calculated waveforms nicely agree.

The performance of the multiharmonic vector rf control is promising. The beam loading compensation up to $h = 8$ with the vector rf control is foreseen. Also, the third ($h = 6$) and fourth ($h = 8$) harmonic voltages in addition to the existing dual harmonic operation may improve the performance of the bunch shaping to alleviate the space charge effects.

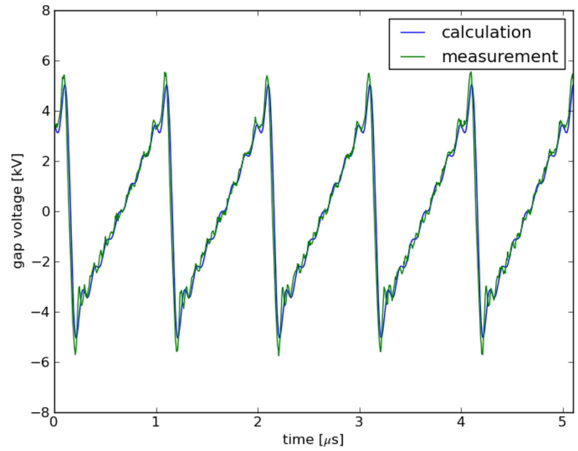

Fig. 15. Comparison of the measured and calculated cavity gap voltage waveforms.

B. High speed serial communication and vector sum function

To examine the high speed serial communication and vector sum function, an I/Q signal rotated by a phase θ for the selected harmonic ($h = 1$) is sent from the cavity driver module to the high speed serial communication module. The normalized vector sum I/Q signal is sent to the common function module. A 4 m long cable is used as the DUT for this test.

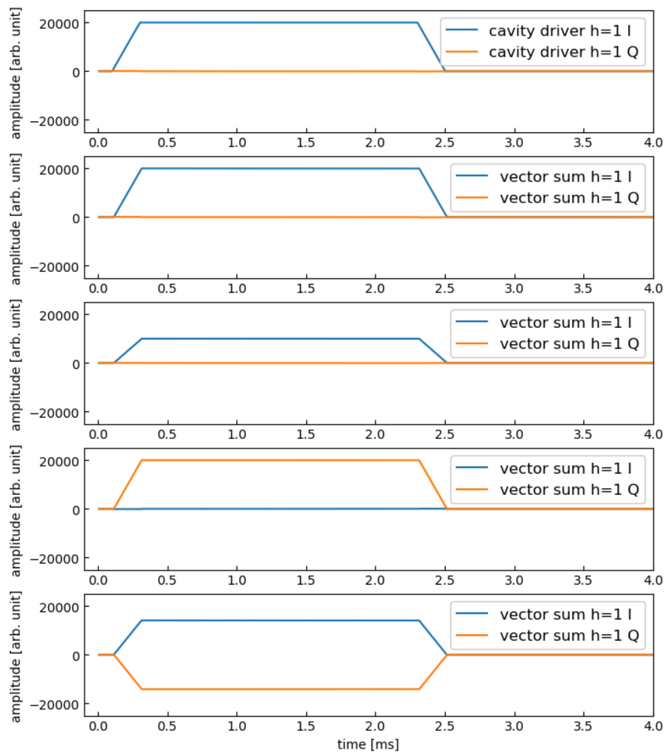

Fig. 16. I/Q waveforms. The top is the I/Q signal measured by the cavity driver. The others are received vector sum signals at the common function module. From the second top to the bottom, the signal normalized by 1 without rotation, the signal normalized by factor of 2 without rotation, the signal normalized by 1 with the rotation angle of 90 degrees, and the signal normalized by 1 with the rotation angle of -45 degrees.

The top plot of Fig. 16 shows the measured I/Q signal at the cavity driver module. The amplitude of I is 20000 and the Q is zero. The envelope is a trapezoid. The rising and falling time is 0.2 ms and the flattop width is 2 ms.

The other plots in Fig. 16 are received vector sum signals at the common function module. The second top plot shows the signal normalized by 1 without rotation. It is identical to the I/Q signal measured by the cavity driver module. The middle plot shows the signal normalized by factor of 2 without rotation. The amplitude is a half of the original signal.

The second bottom plot show the signal normalized by 1 with the rotation angle of 90 degrees. The amplitude of I is zero and the Q is 20000. The bottom is the signal normalized by 1 with the rotation angle of -45 degrees. The amplitude of I is close to $20000 \times 1/\sqrt{2} = 14142$ and the Q is similar to I with negative sign.

This simple test proves that the vector sum function works correctly as designed. We should note that we did not see any errors on the I/Q waveforms; the high speed serial transfer via the Xilinx Aurora is very stable.

V. Summary and Outlook

We summarize the article as follows.

The existing LLRF control system has been working nicely without major problems for more than ten yeas. However, it will be difficult to maintain the system in near future because of the discontinued FPGAs on the system. The MicroTCA.4 based next generation LLRF control system is now under development.

Similar LLRF functions are to be implemented in the new system with several new features. The key feature of the new system is the multiharmonic vector rf control, which would compensate the heavy beam loading in the wideband rf cavity and can expand the performance of the longitudinal painting injection. With the capability of the MicroTCA.4 backplane for high speed serial communication, the sophisticated signal transfer between the modules is realized.

We will add five cavity driver modules to control twelve cavities and implement the remaining LLRF functions. We plan to replace the existing system with the new system during the summer maintenance period in 2019. Prior to the replacement, we will perform beam tests with the new system mainly focused on the beam loading compensation.

Acknowledgments

We would like to thank Heiko Damerau and John Molendijk for fruitful discussions on LLRF topics. We also would like to thank the J-PARC writing support group, which continuously encouraged us to write up this article. Finally, we would like to thank all the members of the J-PARC.

References

[1] “Accelerator technical design report for J-PARC,” JAERI-TECH 2003-044, 2003.

[2] H. Hotchi, H. Harada, N. Hayashi, S. Kato, M. Kinsho, K. Okabe, P. K. Saha, Y. Shobuda, F. Tamura, N. Tani, Y. Watanabe, K. Yamamoto, M. Yamamoto, and M. Yoshimoto, “Achievement of a low-loss 1-MW beam operation in the 3-GeV rapid cycling synchrotron of the Japan Proton Accelerator Research Complex,” *Phys. Rev. Accel. Beams*, vol. 20, p. 060402, Jun 2017. [Online]. Available: https://link.aps.org/doi/10.1103/PhysRevAccelBeams.20.060402

[3] F. Pedersen, “Beam loading effects in the CERN PS booster,” *IEEE Trans. Nucl. Sci.*, vol. 22, no. CERN-MPS-Int-BR-75-6. 3, pp. 1906–1909, Mar 1975.

[4] F. Tamura, A. Schnase, and M. Yoshii, “Dual-harmonic auto voltage control for the rapid cycling synchrotron of the Japan Proton Accelerator Research Complex,” *Phys. Rev. ST Accel. Beams*, vol. 11, no. 7, p. 072001, Jul 2008.

[5] F. Tamura *et al.*, “Longitudinal painting with large amplitude second harmonic rf voltages in the rapid cycling synchrotron of the Japan Proton Accelerator Research Complex,” *Phys. Rev. ST Accel. Beams*, vol. 12, no. 4, p. 041001, Apr 2009.

[6] F. Tamura, M. Yamamoto, C. Ohmori, A. Schnase, M. Yoshii, M. Nomura, M. Toda, T. Shimada, K. Hara, and K. Hasegawa, “Multiharmonic rf feedforward system for beam loading compensation in wide-band cavities of a rapid cycling synchrotron,” *Phys. Rev. ST Accel. Beams*, vol. 14, p. 051004, May 2011. [Online]. Available: http://link.aps.org/doi/10.1103/PhysRevSTAB.14.051004

[7] F. Tamura, H. Hotchi, A. Schnase, M. Yoshii, M. Yamamoto, C. Ohmori, M. Nomura, M. Toda, T. Shimada, K. Hasegawa, and K. Hara, “High intensity single bunch operation with heavy periodic transient beam loading in wide band rf cavities,” *Phys. Rev. ST Accel. Beams*, vol. 18, p. 091004, Sep 2015. [Online]. Available: http://link.aps.org/doi/10.1103/PhysRevSTAB.18.091004